

Review

# The Neutron Macromolecular Crystallography Instruments at Oak Ridge National Laboratory: Advances, Challenges, and Opportunities

Flora Meilleur<sup>1,2,\*</sup>, Leighton Coates<sup>1,\*</sup>, Matthew J. Cuneo<sup>1,3</sup>, Andrey Kovalevsky<sup>1</sup> and Dean A. A. Myles<sup>1</sup>

<sup>1</sup> Neutron Scattering Division, Oak Ridge National Laboratory, Oak Ridge, TN 37831, USA; Matt.Cuneo@stjude.org (M.J.C.); kovalevskyay@ornl.gov (A.K.); mylesda@ornl.gov (D.A.A.M.)

<sup>2</sup> Department of Molecular and Structural Biochemistry, North Carolina State University, Raleigh, NC 27695, USA

<sup>3</sup> Department of Structural Biology, St. Jude Children's Research Hospital, Memphis, TN 38105, USA

\* Correspondence: fmeilleur@ncsu.edu or meilleurf@ornl.gov (F.M.); coatesl@ornl.gov (L.C.); Tel.: +1-865-576-2779 (F.M.); +1-865-574-4620 (L.C.)

Received: 25 September 2018; Accepted: 5 October 2018; Published: 11 October 2018



**Abstract:** The IMAGINE and MaNDi instruments, located at Oak Ridge National Laboratory High Flux Isotope Reactor and Spallation Neutron Source, respectively, are powerful tools for determining the positions of hydrogen atoms in biological macromolecules and their ligands, orienting water molecules, and for differentiating chemical states in macromolecular structures. The possibility to model hydrogen and deuterium atoms in neutron structures arises from the strong interaction of neutrons with the nuclei of these isotopes. Positions can be unambiguously assigned from diffraction studies at the 1.5–2.5 Å resolutions, which are typical for protein crystals. Neutrons have the additional benefit for structural biology of not inducing radiation damage to protein crystals, which can be critical in the study of metalloproteins. Here we review the specifications of the IMAGINE and MaNDi beamlines and illustrate their complementarity. IMAGINE is suitable for crystals with unit cell edges up to 150 Å using a quasi-Laue technique, whereas MaNDi provides neutron crystallography resources for large unit cell samples with unit cell edges up to 300 Å using the time of flight (TOF) Laue technique. The microbial culture and crystal growth facilities which support the IMAGINE and MaNDi user programs are also described.

**Keywords:** neutron; crystallography; macromolecules; Laue diffraction; hydrogen; proton; deuteration

## 1. Introduction

Neutron diffraction is directly analogous to X-ray diffraction, but the information that is derived on molecular structure differs in several critical respects. Neutrons interact with nuclei, while X-rays interact with electrons, and neutron scattering lengths ( $b$ ) show little uniformity across the periodic table [1]. This is in marked contrast to X-ray diffraction, where the strength of scattering depends directly on the atomic number ( $Z$ ) of an atom (Table 1). As a result, atoms that are difficult to resolve in X-ray structural analysis may be more readily distinguished in a complementary neutron analysis. Most importantly for studies of biological systems, neutrons are extremely sensitive to hydrogen and its isotope, deuterium. In addition, neutrons are uncharged, have low thermal energies (0.1–10 meV), and are, thus, gentle non-ionizing probes that easily penetrate fragile biological materials without causing radiation damage.

At the atomic level, neutron diffraction is uniquely able to determine the location of individual hydrogen atoms in biological materials. This provides fundamental insight and mechanistic

understanding of, for example, catalytic processes in enzymes, or of the proton shuttling/relay pathways involved in biological processes [2]. A major limitation, however, is that the inherent flux of neutron beams ( $10^6$ – $10^8$  neutrons  $\text{cm}^{-2} \text{s}^{-1}$ ) is orders of magnitude less than conventional X-ray beams, requiring larger crystals ( $>0.1 \text{ mm}^3$ ) and extended data collection times (days or weeks) compared to those typical for X-ray analysis. In this paper we review the capabilities of the IMAGINE and MaNDi single-crystal neutron diffractometers installed at the Oak Ridge national Laboratory (ORNL) High Flux Isotope Reactor (HFIR) and Spallation Neutron Source (SNS), respectively. The progression in unit cell size that can be efficiently studied by IMAGINE ( $10^6 \text{ \AA}^3$ ) and MaNDi ( $10^7 \text{ \AA}^3$ ) combined with on-site protein crystal growth and deuteration facilities is enabling a broad range of neutron single-crystal studies of complex biological systems.

**Table 1.** Neutron scattering lengths and X-ray scattering factors for atoms in biological macromolecules.

	H	D	C	N	O
Neutron coherent scattering length ( $10^{-12} \text{ cm}$ )	−0.374	0.667	0.665	0.936	0.581
Neutron incoherent cross section (Barns)	80.27	2.05	0	0.49	0
X-ray Scattering Factors ( $10^{-12} \text{ cm}$ ) $\sin\theta/\lambda = 0$	0.28	0.28	1.69	1.97	2.25
X-ray Scattering Factors ( $10^{-12} \text{ cm}$ ) $\sin\theta/\lambda = 0.5 \text{ \AA}^{-1}$	0.02	0.02	0.48	0.53	0.62

## 2. High Flux Isotope Reactor Cold Guide 4D, IMAGINE

The IMAGINE diffractometer is installed on the end-station of cold guide number 4 (CG4-D) at the HFIR. This position has a flux of  $2 \times 10^9 \text{ n/s/cm}^2$  over the useful 2–10  $\text{\AA}$  wavelength range. The instrument receives neutrons from a  $19 \times 12 \text{ mm}^2$  section of the CG4 guide. The neutron wavelength and bandpass delivered to the sample can be varied remotely by motorized translation of three neutron flat mirrors and three pairs of neutron filters that provide short wavelength ( $\lambda_{\text{min}} = 2.0, 2.8, \text{ and } 3.3 \text{ \AA}$ ) and long wavelength ( $\lambda_{\text{max}} = 3.0, 4.0, \text{ and } 4.5 \text{ \AA}$ ) cut-offs, respectively. A pair of elliptically-shaped mirrors then collects and focuses the resulting beam vertically and horizontally down to  $2 \times 3.2 \text{ mm}^2$  at the sample position, with full width vertical and horizontal divergence of  $0.5^\circ$  and  $0.6^\circ$ , respectively, and delivery of  $\sim 3 \times 10^7 \text{ n/s/cm}^2$  in standard 2.8–4.0  $\text{\AA}$  quasi-Laue configuration [2,3]. Complete specifications of the IMAGINE instrument are listed in Table 2. IMAGINE is equipped with a neutron sensitive image plate detector [4]. The cylindrical image plate detector has high-efficiency, high spatial resolution, and provides good reciprocal space coverage on a continuous surface, reaching out to  $\sim 1.1 \text{ \AA}$  resolution.

**Table 2.** Specifications of the neutron protein crystallography instrumentation available to external users at Oak Ridge National Laboratory.

	IMAGINE (HFIR, ORNL)	MANDI (SNS, ORNL)
Neutron Source	Reactor	Spallation Source
Moderator	Hydrogen cold source	Decoupled hydrogen
Source frequency	n/a	60 Hz
Avg. Flux	$\sim 3 \times 10^7 \text{ n/s/cm}^2$ (2.8–4.0 $\text{\AA}$ )	$\sim 2.06 \times 10^7 \text{ n/s/cm}^2$
Flight Path	13 m downstream CTAX instrument	30 m
Beam size	$3.2 \times 2.0 \text{ mm}^2$	Variable diameter pin holes: 1.0–6.0 mm
Scattering angles	Horizontal: $\pm 151^\circ$ Vertical: $\pm 48^\circ$	$4 \pi$
Optics	Flat mirrors, wavelength selection filters, Elliptic focusing mirrors &	Bandwidth Choppers, Mirrors
Incident $\lambda$	2–10 $\text{\AA}$	1–10 $\text{\AA}$
$\Delta \lambda/\lambda$	25%	2.15 $\text{\AA}$ or 4.3 $\text{\AA}$ window 0.4% resolution (TOF)
Detector type	Neutron Image Plate	SNS Anger Camera

Table 2. Cont.

	IMAGINE (HFIR, ORNL)	MANDI (SNS, ORNL)
No. of detectors	1 $\frac{1}{2}$	40
Detector active area	1200 $\times$ 450 mm <sup>2</sup>	40 detectors (150 $\times$ 150 mm <sup>2</sup> )
Detector solid angle	7.85 sr	4.1 sr
Crystal size (protein)	>0.3 mm <sup>3</sup>	>0.1 mm <sup>3</sup>
Unit cell dimension	<150 Å	<300 Å

The IMAGINE neutron image plate diffractometer is designed for rapid collection of high-resolution quasi-Laue data from small single crystals (>0.3 mm<sup>3</sup>) of moderate unit cell size (<150 Å). The IMAGINE diffractometer has served the structural biology community since entering the ORNL user program in 2013. However, the tunability of the optics and the recent development of extreme sample environment capabilities give the instrument the potential of serving diverse scientific user communities for the analysis of light atom positions in materials that are of interest across the fields of structural biology, pharmacology, chemistry, condensed matter physics, nano-structured materials and geological sciences [5]. In 2016, the instrument was equipped with a custom closed cycle refrigerator (CCR) covering a temperature range from 4.5 K to 400 K. The CCR enables parametric studies of magnetic and supramolecular structures, of incommensurate systems, and of phase transitions in soft condensed matter materials. It also provides cryo-cooling capabilities for macromolecular crystallography, which will enable data collection on enzyme samples with trapped intermediates whose room-temperature lifetime are too short to analyze structurally [6,7].

### 3. Spallation Neutron Source Beam Line 11B, MaNDi

The macromolecular neutron diffractometer (MaNDi) is situated at the first target station of the SNS [8]. The instrument is designed to collect neutron diffraction data from small single crystals (>0.1 mm<sup>3</sup>) with lattice constants between 10 and 300 Å [9]. A focusing neutron guide has been designed to filter the high-energy neutron component of the spectrum and to provide a narrow beam with a wide spectral window and angular divergence almost insensitive to neutron wavelength [10]. The neutron guide starts 6 m from the decoupled hydrogen moderator and three bandwidth choppers are located at 6.2, 7.2 and 10.5 m from the moderator. The chopper system delivers a wavelength bandwidth  $\Delta\lambda = 2.15$  or 4.3 Å, which can be selected anywhere between 1–10 Å. The instrument includes a final interchangeable section of neutron guide and two slits, which can be used to alter the horizontal and vertical beam divergence between 0.12 and 0.80 (full width at half-maximum) at the sample position. This allows users to trade intensity for resolution, depending on the experimental requirements. The sample position is surrounded by a spherical detector array frame (DAF) which is currently populated with 40 out of a total of 46 possible SNS Anger camera detectors. The sample-to-detector distance varies from 39 to 45 cm currently giving a detector coverage of over 4 sr. The instrument goniometer is raised from the top of the DAF for sample loading. After a sample has been mounted, the diffraction goniometer translates downwards to interlock with a set of kinematic mounts on top of the DAF by a motorized goniometer lifting and lowering mechanism. Complete specifications of the MaNDi instrument are detailed in Table 2.

The MaNDi instrument entered the general user program in 2014. Data are typically collected at room temperature using capillary mounted crystals. An Oxford diffraction cryostream system provides an experimental temperature range of 80 to 400 K, which enables standard cryo-crystallography pins and loops to be used for data collection [11]. Cryogenic neutron data collection enables the study of transient protein ligand complexes and is in increasing demand.

#### 4. Software

The software packages used for data reduction and refinement on IMAGINE and MaNDi are summarized in Table 3. While the data collection and reduction packages differ at each beamline, the reduced neutron datasets from all beam lines are compatible with standard user community packages for crystallographic analysis (Phenix.refine, SHELX, nCNS) and modelling (Coot) [12–15]. For indexing and integration, IMAGINE uses the LAUEGEN suite of software, which was developed originally for X-ray Laue crystallography and then adapted for neutron diffraction and cylindrical detector geometries [16,17]. MaNDi uses the Mantidplot [18] suite of programs to calibrate detectors, find peaks, find UB matrices, choose the symmetry of the unit cell, index peaks, integrate peaks, and visualize the data. These algorithms have been combined in a single crystal diffraction Event Data Reduction Interface for automated use [19]. Profile fitting method for peak integration was recently developed and implemented Wavelength normalization [20] is performed with Lscale and Lauenorm on IMAGINE and MaNDi, respectively [21,22]. SCALA from the CCP4 suite of programs can be used to scale and merge the data [23].

The CrystalPlan software package allows users to optimize data collection strategies, and maximize the efficient use of available beam time [24]. The goniometer settings are optimized using a genetic algorithm that starts with a population of random goniometer settings and finds combinations that maximize reciprocal space coverage and data completeness in the minimal number of frames. For example, in the case of carbonic anhydrase (P2<sub>1</sub>) on MaNDi, comparison of data collected 10-degree increments about a single rotation axis with those optimized by CrystalPlan shows that the coverage increased from 62% to 82%, a gain of 20% for this crystal. With T4 lysozyme (P3<sub>2</sub>21), collecting 10 data frames in 10° steps about a single axis results in 74% coverage, whereas collecting 10 frames in optimized orientations result in 87% coverage. CrystalPlan is fully integrated on MaNDi and will be interfaced with a kappa goniometer head on IMAGINE in 2018.

**Table 3.** Data reduction and refinement software used on IMAGINE, MaNDi.

	CG-4D (IMAGINE)	MANDI (SNS, ORNL)
Data collection	Arinax GUI	SNS software CSS (EPICS)
Data collection strategy	CrystalPlan (in 2018t)	CrystalPlan
Data reduction	Lauegen, Lscale, SCALA/AIMLESS	Mantid, Lauenorm, SCALA/AIMLESS
Data visualization	ARINAX GUI, ImageJ	Mantid
Data analysis packages	Phenix.refine, SHELX, nCNS	
Data Modeling	Coot	
Computing resources	PC and Linux	

#### 5. Protein Preparation and Crystal Growth

Neutron macromolecular crystallography remains a challenging experimental technique but provides unique information on H atoms that is often not accessible by other methods. One complication is that hydrogen also gives rise to a large incoherent neutron scattering background that limits the resolution of the data [25]. Since protein crystals typically contain ~50% solvent, this can be remedied, in part, by replacing H<sub>2</sub>O with D<sub>2</sub>O in the crystal. Total replacement of hydrogen by deuterium (perdeuteration) can be achieved by over expressing the protein in deuterated media [26]. Perdeuteration reduces the sample background by a factor of 40, enabling faster and more accurate data collection from smaller samples, and improving the quality of the neutron scattering length density maps. However, deuteration can also alter the hydrophobicity of a protein surface, interfering with crystal growth. Partial deuteration, using 100% D<sub>2</sub>O but hydrogenous carbon sources in expression media, results in ~80–85% after H/D exchange and has helped in several cases [27–29].

ORNL provides user access to specialized facilities for the production of perdeuterated proteins and for growth of large (>0.1 mm<sup>3</sup>) neutron quality crystals [30]. The Biodeuteration Laboratory supports large-scale (up to 5 L) high cell density growth of *Escherichia coli* and yeast in hydrogenated and deuterated culture media as well as small-scale (200 mL) fermentations for optimization [26].

The crystallization laboratory is equipped with biophysical characterization equipment, including a dynamic light scattering instrument, a circular dichroism spectropolarimeter, fluorescence microscope and stereomicroscopes, a Gryphon crystallization robot and a Scorpion liquid dispensing robot, and 13 temperature-controlled chambers and other devices for crystallogensis and large crystal growth. An X-ray laboratory is equipped with a Rigaku high intensity micro-focus rotating anode X-ray generator, with one port outfitted for macromolecular crystallography while the other port is occupied by a Bio-SAXS small angle scattering instrument.

## 6. IMAGINE and MaNDi Complementarity

The IMAGINE and MANDI beamlines are designed to meet the complementary demands of capacity and capability. IMAGINE is designed for rapid collection (hours-days) of high resolution ( $\sim 1.1$  Å) Laue or quasi-Laue data from small single crystals (supra molecules:  $< 0.05$  mm<sup>3</sup>; proteins:  $> 0.3$  mm<sup>3</sup>) of moderately large unit cell size ( $< 150$  Å). By contrast, MaNDi is designed to collect high resolution ( $\sim 1.0$  Å) data on samples of  $0.1$  mm<sup>3</sup> from the most challenging unit cells systems, ( $> 150$ – $300$  Å), and is, thus, uniquely able to analyze much larger and more complex proteins and assemblies that are beyond the range of IMAGINE and other neutron facilities. While the capabilities of both instruments overlap for mid-range systems, IMAGINE provides work horse capacity for data collection, while MANDI provides unique capability for the most challenging and demanding systems.

The macromolecule structures deposited in the Protein Data Bank and solved against neutron crystallographic data collected on IMAGINE and MaNDi are listed in Tables 4 and 5, respectively.

**Table 4.** Protein structures solved using the IMAGINE instrument. DHFR, dihydrofolate reductase. MTAN, 5'-methylthioadenosine nucleosidase. LPMO, lytic polysaccharide monooxygenase. ConA, Concanavalin A. \* The primitive unit cell volumes were computed using the online calculator [31].

Protein	PDB ID	Primitive Unit Cell Volume (Å <sup>3</sup> ) *	Crystal Volume (mm <sup>3</sup> )	Reference
Rubredoxin	4K9F	51,030	0.7	[3]
DHFR	4PDJ	154,857	3.6	[32,33]
RAS GTPase	4RSG	223,731	0.7	[34]
		405,350		
MTAN	5CCD 5JPC 5K1Z	405,350	1.5	[28]
		405,350		
Carbonic Anhydrase	5C8I	126,464	0.7	[35]
HIV protease	5E5K	241,373	0.5	[29]
Cholesterol Oxidase	5KWF	235,475	0.4	[36]
LPMO (9)	5TKI	200,072	0.3	[37,38]
T4 Lysozyme	5VNQ	314,129	0.7	[6]
T4 Lysozyme	5XPE	314,270	0.9	[7]
ConA	5WEY	264,656	1	[39]

**Table 5.** Protein structure solved using the MaNDi instrument. IPP, Inorganic Pyrophosphatase. LPMO, lytic polysaccharide monooxygenase. AAC, aminoglycoside acetyltransferase. MnSOD, manganese superoxide dismutase. FMO, Fenna-Matthews-Olson complex. RSFP, reversibly switchable fluorescent protein. CA-EZM, carbonic anhydrase in complex with ethoxzolamide. CA-DZM, carbonic anhydrase in complex with dorzolamide.

Protein	PDB ID	Primitive Unit Cell Volume (Å <sup>3</sup> )	Crystal Volume (mm <sup>3</sup> )	Reference
Xylanase	4S2F	210,271	3	[40]
Toho1 $\beta$ -lactamase	5A93	460,246	0.4	[41]
Dathail (RSFP)	5EBJ	259,041	10	[42]
Toho1 $\beta$ -lactamase	5KSC	461,045	0.9	[43]

Table 5. Cont.

Protein	PDB ID	Primitive Unit Cell Volume ( $\text{\AA}^3$ )	Crystal Volume ( $\text{mm}^3$ )	Reference
Chlorite dismutase	5NKU	132,679	0.8	[44]
IPP	5TY5	565,529	6	Unpublished
LPMO (10)	5VG1	303,571	2.7	[45,46]
AAC	6BBR	174,616	0.4	[47]
	6BBZ	167,851	0.4	[47]
CA-EZM	6BCC	125,909	0.6	[27]
CA-DZM	6BC9	126,768	0.6	[27]
Toho1 $\beta$ -lactamase	6C78	463,740	Not measured	[48]
Galectin	6EYM	137,845	1.0	[49,50]
tRNA hydrolase	Not yet deposited	571,442	0.15	[8]
MnSOD	Not yet deposited	1,385,615	0.26	[51]
FMO	Not yet deposited	595,262	0.3	Lu et al., 2018, Acta Crystallographica E, under review
Photosystem II subunit PsbO	Not Yet Deposited	527,955	0.25	[52]

Figure 1 plots the volume of crystals used for data collection on IMAGINE and MaNDi against the volume of the primitive unit cell. The average diffracted intensity is proportional to the volume of the crystal,  $V$ , and inversely proportional to the square of the primitive unit cell volume,  $v_0$ , while the number and density of reflections is directly related to the unit cell volume and the resolution of the data. As the tables and Figure 1 show, both instruments are pushing the limits of minimum crystal size unit cell needed for neutron single-crystal diffraction, which traditionally has been a limitation of this method. On IMAGINE, spatial overlap and deconvolution of reflections becomes limiting for systems with primitive unit cell volumes greater than  $\sim 450,000 \text{ \AA}^3$ . By contrast, on MaNDi, the fine time-of-flight wavelength resolution (0.4%) enables the dense diffraction patterns from much larger unit cell ( $>150 \text{ \AA}$ ) systems to be resolved. However, as the average diffracted intensity depends upon the  $V/v_0^2$  ratio, analyzing these larger unit cell systems necessarily requires more beam time days. SNS operates  $\sim 200$  days/annum, which enables MaNDi to tackle these more challenging problems and sets new horizons for spallation neutron crystallography. HFIR operates 165 days/annum, which enables IMAGINE to perform as a data collection workhorse.

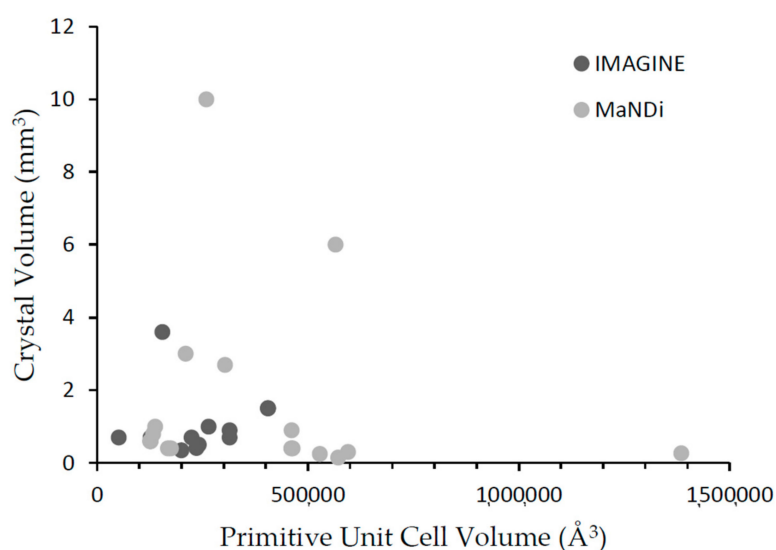


**Figure 1.** Volume of the crystals used for data collection on IMAGINE and MaNDi plotted against the volume of the primitive unit cell.

## 7. Future Developments

IMAGINE can collect data from macromolecular, supramolecular, and small molecule materials crystals. The addition of closed cycle refrigerator (CCR) in 2016 that covers a temperature range from 4.5 K to 400 K now enables parametric studies of magnetic and supramolecular structures, of incommensurate systems, and of phase transitions in condensed matter materials. It also provides cryo-cooling capabilities for macromolecular crystallography, which will enable data collection on enzyme samples with trapped intermediates whose room-temperature lifetime is too short to analyze structurally [6,7]. In 2018, the first experiments using a new diamond cell that is optimized for single-crystal neutron diffraction and capable of achieving pressures of ~20 GP, demonstrated the potential to develop a new program of high-pressure science on the instrument [5].

Longer term, the planned 2022 replacement of the ender section located downstream of the HFIR cold source, which is known to be compromised, and upgrade of the front end of the CG-4 cold guide system will deliver a two- to four-fold increase in flux on the instrument.

MaNDi is uniquely placed in the global neutron crystallography community as a TOF-resolved Laue diffractometer for very large (>150 Å) unit cell systems. The switch from H<sub>2</sub>O to D<sub>2</sub>O in the moderator cooling system at the SNS in 2018 has increased the incident flux on sample at MaNDi by 30%, lowering the exposure time needed for each orientation. With SNS now operating at 1.4 MW, MaNDi will be able to collect data from smaller, more complex samples, such as membrane proteins and large enzyme complexes. The SNS is currently undergoing a power upgrade project that increase beam power to 2 MW at the first target station, while also paving the way for the construction of an SNS second target station (STS). The high brightness of the proposed neutron moderators at the STS are ideally matched to experiments utilizing small samples such as protein crystallography. The Ewald single crystal instrument proposed at STS will deliver a 60× increase in the flux available on MaNDi [53]. Thus, IMAGINE and MaNDi will continue to offer outstanding capabilities in the decade ahead, with current and near-term upgrades that are expected to deliver further significant enhancements in flux opening the way to new areas of science and more challenging studies ahead.

**Author Contributions:** Writing-Original Draft Preparation, F.M., L.C., M.J.C., A.K., D.A.A.M.; Writing-Review & Editing, F.M.

**Funding:** This research was funded by the National Science Foundation grant number 0922719.

**Acknowledgments:** This research used resources at the High Flux Isotope Reactor and Spallation Neutron Source, a DOE Office of Science User Facility operated by the Oak Ridge National Laboratory. F.M. acknowledge support from the USDA National Institute of Food and Agriculture, Hatch project 1010523. The installation of the IMAGINE instrument was supported in part by the National Science Foundation award 0922719.

**Conflicts of Interest:** The authors declare no conflict of interest.

## References

1. Neutron Scattering Lengths and Cross Sections. Available online: <https://www.nist.gov/ncnr/planning-your-experiment/sld-periodic-table> (accessed on 10 October 2018).
2. Schroder, G.C.; O'Dell, W.B.; Myles, D.A.A.; Kovalevsky, A.; Meilleur, F. Imagine: Neutrons reveal enzyme chemistry. *Acta Crystallogr. D Biol. Crystallogr.* **2018**, *74*, 778–786. [CrossRef] [PubMed]
3. Meilleur, F.; Munshi, P.; Robertson, L.; Stoica, A.D.; Crow, L.; Kovalevsky, A.; Koritsanszky, T.; Chakoumakos, B.C.; Blessing, R.; Myles, D.A. The imagine instrument: First neutron protein structure and new capabilities for neutron macromolecular crystallography. *Acta Crystallogr. D Biol. Crystallogr.* **2013**, *69*, 2157–2160. [CrossRef] [PubMed]
4. Wilkinson, C.; Lehmann, M.S.; Meilleur, F.; Blakeley, M.P.; Myles, D.A.A.; Vogelmeier, S.; Thoms, M.; Walsh, M.; McIntyre, G.J. Characterization of image plates for neutron diffraction. *J. Appl. Crystallogr.* **2009**, *42*, 749–757. [CrossRef]
5. Haberl, B.; Dissanayake, S.; Wu, Y.; Myles, D.A.A.; Dos Santos, A.M.; Loguillo, M.; Rucker, G.M.; Armitage, D.P.; Cochran, M.; Andrews, K.M.; et al. Next-generation diamond cell and applications to single-crystal neutron diffraction. *Rev. Sci. Instrum.* **2018**, *89*, 092902. [CrossRef] [PubMed]

6. Li, L.; Shukla, S.; Meilleur, F.; Standaert, R.F.; Pierce, J.; Myles, D.A.A.; Cuneo, M.J. Neutron crystallographic studies of t4 lysozyme at cryogenic temperature. *Protein Sci.* **2017**, *26*, 2098–2104. [[CrossRef](#)] [[PubMed](#)]
7. Hiromoto, T.; Meilleur, F.; Shimizu, R.; Shibasaki, C.; Adachi, M.; Tamada, T.; Kuroki, R. Neutron structure of the T26H mutant of T4 phage lysozyme provides insight into the catalytic activity of the mutant enzyme and how it differs from that of wild type. *Protein Sci.* **2017**, *26*, 1953–1963. [[CrossRef](#)] [[PubMed](#)]
8. Coates, L.; Cuneo, M.J.; Frost, M.J.; He, J.H.; Weiss, K.L.; Tomanicek, S.J.; McFeeters, H.; Vandavasi, V.G.; Langan, P.; Iverson, E.B. The macromolecular neutron diffractometer mandi at the spallation neutron source. *J. Appl. Crystallogr.* **2015**, *48*, 1302–1306. [[CrossRef](#)]
9. Schultz, A.J.; Thiyagarajan, P.; Hodges, J.P.; Rehm, C.; Myles, D.A.A.; Langan, P.; Mesecar, A.D. Conceptual design of a macromolecular neutron diffractometer (MaNDi) for the SNS. *J. Appl. Crystallogr.* **2005**, *38*, 964–974. [[CrossRef](#)]
10. Coates, L.; Stoica, A.D.; Hoffmann, C.; Richards, J.; Cooper, R. The macromolecular neutron diffractometer (MaNDi) at the Spallation Neutron Source, Oak Ridge: Enhanced optics design, high-resolution neutron detectors and simulated diffraction. *J. Appl. Crystallogr.* **2010**, *43*, 570–577. [[CrossRef](#)]
11. Coates, L.; Tomanicek, S.; Schrader, T.E.; Weiss, K.L.; Ng, J.D.; Juttner, P.; Ostermann, A. Cryogenic neutron protein crystallography: Routine methods and potential benefits. *J. Appl. Crystallogr.* **2014**, *47*, 1431–1434. [[CrossRef](#)]
12. Afonine, P.V.; Mustyakimov, M.; Grosse-Kunstleve, R.W.; Moriarty, N.W.; Langan, P.; Adams, P.D. Joint X-ray and neutron refinement with phenix.Refine. *Acta Crystallogr. D Biol. Crystallogr.* **2010**, *66*, 1153–1163. [[CrossRef](#)] [[PubMed](#)]
13. Gruene, T.; Hahn, H.W.; Luebben, A.V.; Meilleur, F.; Sheldrick, G.M. Refinement of macromolecular structures against neutron data with Shelx12013. *J. Appl. Crystallogr.* **2014**, *47*, 462–466. [[CrossRef](#)] [[PubMed](#)]
14. *104 Patch for CNS*; nCNS an Open Source Distribution Patch for CNS Macromolecular Structure Refinement; Los Alamos National Security: Los Alamos, NM, USA, 2007.
15. Emsley, P.; Lohkamp, B.; Scott, W.G.; Cowtan, K. Features and development of coot. *Acta Crystallogr. D Biol. Crystallogr.* **2010**, *66*, 486–501. [[CrossRef](#)] [[PubMed](#)]
16. Campbell, J.W. Lauegen, an X-windows-based program for the processing of laue X-ray-diffraction data. *J. Appl. Crystallogr.* **1995**, *28*, 228–236. [[CrossRef](#)]
17. Campbell, J.W.; Hao, Q.; Harding, M.M.; Nguti, N.D.; Wilkinson, C. Lauegen version 6.0 and INTLDM. *J. Appl. Crystallogr.* **1998**, *31*, 496–502. [[CrossRef](#)]
18. Arnold, O.; Bilheux, J.C.; Borreguero, J.M.; Buts, A.; Campbell, S.I.; Chapon, L.; Doucet, M.; Draper, N.; Leal, R.F.; Gigg, M.A.; et al. Mantid-data analysis and visualization package for neutron scattering and mu sr experiments. *Nucl. Instrum. Meth. A* **2014**, *764*, 156–166. [[CrossRef](#)]
19. Schultz, A.J.; Jorgensen, M.R.V.; Wang, X.P.; Mikkelsen, R.L.; Mikkelsen, D.J.; Lynch, V.E.; Peterson, P.F.; Green, M.L.; Hoffmann, C.M. Integration of neutron time-of-flight single-crystal bragg peaks in reciprocal space. *J. Appl. Crystallogr.* **2014**, *47*, 915–921. [[CrossRef](#)]
20. Sullivan, B.; Archibald, R.; Langan, P.S.; Dobbek, H.; Bommer, M.; McFeeters, R.L.; Coates, L.; Wang, X.P.; Gallmeier, F.; Carpenter, J.M.; et al. Improving the accuracy and resolution of neutron crystallographic data by three-dimensional profile fitting of Bragg peaks in reciprocal space. *Acta Crystallogr. Sect. D* **2018**. Accepted.
21. Arzt, S.; Campbell, J.W.; Harding, M.M.; Hao, Q.; Helliwell, J.R. Lscale—The new normalization, scaling and absorption correction program in the daresbury laue software suite. *J. Appl. Crystallogr.* **1999**, *32*, 554–562. [[CrossRef](#)]
22. Helliwell, J.R.; Habash, J.; Cruickshank, D.W.J.; Harding, M.M.; Greenhough, T.J.; Campbell, J.W.; Clifton, I.J.; Elder, M.; Machin, P.A.; Papiz, M.Z.; et al. The recording and analysis of synchrotron X-radiation laue diffraction photographs. *J. Appl. Crystallogr.* **1989**, *22*, 483–497. [[CrossRef](#)]
23. Winn, M.D.; Ballard, C.C.; Cowtan, K.D.; Dodson, E.J.; Emsley, P.; Evans, P.R.; Keegan, R.M.; Krissinel, E.B.; Leslie, A.G.W.; McCoy, A.; et al. Overview of the ccp4 suite and current developments. *Acta Crystallogr. D Biol. Crystallogr.* **2011**, *67*, 235–242. [[CrossRef](#)] [[PubMed](#)]
24. Zikovskiy, J.; Peterson, P.F.; Wang, X.P.P.; Frost, M.; Hoffmann, C. Crystalplan: An experiment-planning tool for crystallography. *J. Appl. Crystallogr.* **2011**, *44*, 418–423. [[CrossRef](#)]
25. O'Dell, W.B.; Bodenheimer, A.M.; Meilleur, F. Neutron protein crystallography: A complementary tool for locating hydrogens in proteins. *Arch. Biochem. Biophys.* **2016**, *602*, 48–60. [[CrossRef](#)] [[PubMed](#)]

26. Meilleur, F.; Weiss, K.L.; Myles, D.A. Deuterium labeling for neutron structure-function-dynamics analysis. *Methods Mol. Biol.* **2009**, *544*, 281–292. [[PubMed](#)]
27. Kovalevsky, A.; Aggarwal, M.; Velazquez, H.; Cuneo, M.J.; Blakeley, M.P.; Weiss, K.L.; Smith, J.C.; Fisher, S.Z.; McKenna, R. “To be or not to be” protonated: Atomic details of human carbonic anhydrase-clinical drug complexes by neutron crystallography and simulation. *Structure* **2018**, *26*, 383–390. [[CrossRef](#)] [[PubMed](#)]
28. Dajnowicz, S.; Johnston, R.C.; Parks, J.M.; Blakeley, M.P.; Keen, D.A.; Weiss, K.L.; Gerlits, O.; Kovalevsky, A.; Mueser, T.C. Direct visualization of critical hydrogen atoms in a pyridoxal 5'-phosphate enzyme. *Nat. Commun.* **2017**, *8*, 955. [[CrossRef](#)] [[PubMed](#)]
29. Gerlits, O.; Wymore, T.; Das, A.; Shen, C.H.; Parks, J.M.; Smith, J.C.; Weiss, K.L.; Keen, D.A.; Blakeley, M.P.; Louis, J.M.; et al. Long-range electrostatics-induced two-proton transfer captured by neutron crystallography in an enzyme catalytic site. *Angew. Chem. Int. Ed.* **2016**, *55*, 4924–4927. [[CrossRef](#)] [[PubMed](#)]
30. Bio Deuteration Laboratory. Available online: <https://www.ornl.gov/facility/csmb/subpage/bio-deuteration-laboratory> (accessed on 10 October 2018).
31. Karen, V.L.; Mighell, A.D. Perform NIST\*LATTICE Computations. Available online: <https://services.mbi.ucla.edu/nist/> (accessed on 25 September 2018).
32. Wan, Q.; Bennett, B.C.; Wilson, M.A.; Kovalevsky, A.; Langan, P.; Howell, E.E.; Dealwis, C. Toward resolving the catalytic mechanism of dihydrofolate reductase using neutron and ultrahigh-resolution X-ray crystallography. *Proc. Natl. Acad. Sci. USA* **2014**, *111*, 18225–18230. [[CrossRef](#)] [[PubMed](#)]
33. Wan, Q.; Kovalevsky, A.Y.; Wilson, M.A.; Bennett, B.C.; Langan, P.; Dealwis, C. Preliminary joint X-ray and neutron protein crystallographic studies of ecDHFR complexed with folate and NADP+. *Acta Crystallogr. Sect. F Struct. Biol. Cryst. Commun.* **2014**, *70*, 814–818. [[CrossRef](#)] [[PubMed](#)]
34. Knihtila, R.; Holzapfel, G.; Weiss, K.; Meilleur, F.; Mattos, C. Neutron crystal structure of RAS GTPase puts in question the protonation state of the GTP gamma-phosphate. *J. Biol. Chem.* **2015**, *290*, 31025–31036. [[CrossRef](#)] [[PubMed](#)]
35. Aggarwal, M.; Kovalevsky, A.Y.; Velazquez, H.; Fisher, S.Z.; Smith, J.C.; McKenna, R. Neutron structure of human carbonic anhydrase II in complex with methazolamide: Mapping the solvent and hydrogen-bonding patterns of an effective clinical drug. *IUCr* **2016**, *3*, 319–325. [[CrossRef](#)] [[PubMed](#)]
36. Golden, E.; Yu, L.J.; Meilleur, F.; Blakeley, M.P.; Duff, A.P.; Karton, A.; Vrieling, A. An extended N-H bond, driven by a conserved second-order interaction, orients the flavin N5 orbital in cholesterol oxidase. *Sci. Rep.* **2017**, *7*, 40517. [[CrossRef](#)] [[PubMed](#)]
37. O'Dell, W.B.; Agarwal, P.K.; Meilleur, F. Oxygen activation at the active site of a fungal lytic polysaccharide monoxygenase. *Angew. Chem. Int. Ed.* **2017**, *56*, 767–770. [[CrossRef](#)] [[PubMed](#)]
38. O'Dell, W.B.; Swartz, P.D.; Weiss, K.L.; Meilleur, F. Crystallization of a fungal lytic polysaccharide monoxygenase expressed from glycoengineered *Pichia pastoris* for X-ray and neutron diffraction. *Acta Crystallogr. Sect. F Struct. Biol. Cryst. Commun.* **2017**, *73*, 70–78. [[CrossRef](#)] [[PubMed](#)]
39. Gerlits, O.O.; Coates, L.; Woods, R.J.; Kovalevsky, A. Mannobiose binding induces changes in hydrogen bonding and protonation states of acidic residues in concanavalin a as revealed by neutron crystallography. *Biochemistry* **2017**, *56*, 4747–4750. [[CrossRef](#)] [[PubMed](#)]
40. Wan, Q.; Parks, J.M.; Hanson, B.L.; Fisher, S.Z.; Ostermann, A.; Schrader, T.E.; Graham, D.E.; Coates, L.; Langan, P.; Kovalevsky, A. Direct determination of protonation states and visualization of hydrogen bonding in a glycoside hydrolase with neutron crystallography. *Proc. Natl. Acad. Sci. USA* **2015**, *112*, 12384–12389. [[CrossRef](#)] [[PubMed](#)]
41. Vandavasi, V.G.; Weiss, K.L.; Cooper, J.B.; Erskine, P.T.; Tomanicek, S.J.; Ostermann, A.; Schrader, T.E.; Ginell, S.L.; Coates, L. Exploring the mechanism of beta-lactam ring protonation in the class a beta-lactamase acylation mechanism using neutron and X-ray crystallography. *J. Med. Chem.* **2016**, *59*, 474–479. [[CrossRef](#)] [[PubMed](#)]
42. Langan, P.S.; Close, D.W.; Coates, L.; Rocha, R.C.; Ghosh, K.; Kiss, C.; Waldo, G.; Freyer, J.; Kovalevsky, A.; Bradbury, A.R. Evolution and characterization of a new reversibly photoswitching chromogenic protein, dathail. *J. Mol. Biol.* **2016**, *428*, 1776–1789. [[CrossRef](#)] [[PubMed](#)]
43. Vandavasi, V.G.; Langan, P.S.; Weiss, K.L.; Parks, J.M.; Cooper, J.B.; Ginell, S.L.; Coates, L. Active-site protonation states in an acyl-enzyme intermediate of a class a beta-lactamase with a monobactam substrate. *Antimicrob. Agents Chemother.* **2017**, *61*, e01636-16. [[CrossRef](#)] [[PubMed](#)]

44. Schaffner, I.; Mlynek, G.; Flego, N.; Puhlinger, D.; Libiseller-Egger, J.; Coates, L.; Hofbauer, S.; Bellei, M.; Furtmuller, P.G.; Battistuzzi, G.; et al. Molecular mechanism of enzymatic chlorite detoxification: Insights from structural and kinetic studies. *ACS Catal.* **2017**, *7*, 7962–7976. [[CrossRef](#)] [[PubMed](#)]
45. Bacik, J.P.; Mekasha, S.; Forsberg, Z.; Kovalevsky, A.Y.; Vaaje-Kolstad, G.; Eijsink, V.G.H.; Nix, J.C.; Coates, L.; Cuneo, M.J.; Unkefer, C.J.; et al. Neutron and atomic resolution X-ray structures of a lytic polysaccharide monoxygenase reveal copper-mediated dioxygen binding and evidence for N-terminal deprotonation. *Biochemistry* **2017**, *56*, 2529–2532. [[CrossRef](#)] [[PubMed](#)]
46. Bacik, J.P.; Mekasha, S.; Forsberg, Z.; Kovalevsky, A.; Nix, J.C.; Cuneo, M.J.; Coates, L.; Vaaje-Kolstad, G.; Chen, J.C.; Eijsink, V.G.; et al. Neutron and high-resolution room-temperature X-ray data collection from crystallized lytic polysaccharide monoxygenase. *Acta Crystallogr. Sect. F Struct. Biol. Cryst. Commun.* **2015**, *71*, 1448–1452. [[CrossRef](#)] [[PubMed](#)]
47. Kumar, P.; Serpersu, E.H.; Cuneo, M.J. A low-barrier hydrogen bond mediates antibiotic resistance in a noncanonical catalytic triad. *Sci. Adv.* **2018**, *4*, eaas8667. [[CrossRef](#)] [[PubMed](#)]
48. Langan, P.S.; Vandavasi, V.G.; Cooper, S.J.; Weiss, K.L.; Ginell, S.L.; Parks, J.M.; Coates, L. Substrate binding induces conformational changes in a class a beta-lactamase that prime it for catalysis. *ACS Catal.* **2018**, *8*, 2428–2437. [[CrossRef](#)]
49. Manzoni, F.; Saraboji, K.; Sprenger, J.; Kumar, R.; Noresson, A.L.; Nilsson, U.J.; Leffler, H.; Fisher, S.Z.; Schrader, T.E.; Ostermann, A.; et al. perdeuteration, crystallization, data collection and comparison of five neutron diffraction data sets of complexes of human galectin-3C. *Acta Crystallogr. D Biol. Crystallogr.* **2016**, *72*, 1194–1202. [[CrossRef](#)] [[PubMed](#)]
50. Manzoni, F.; Wallerstein, J.; Schrader, T.E.; Ostermann, A.; Coates, L.; Akke, M.; Blakeley, M.P.; Oksanen, E.; Logan, D.T. Elucidation of hydrogen bonding patterns in ligand-free, lactose- and glycerol-bound galectin-3C by neutron crystallography to guide drug design. *J. Med. Chem.* **2018**, *61*, 4412–4420. [[CrossRef](#)] [[PubMed](#)]
51. Azadmanesh, J.; Trickle, S.R.; Weiss, K.L.; Coates, L.; Borgstahl, G.E. Preliminary neutron diffraction analysis of challenging human manganese superoxide dismutase crystals. *Acta Crystallogr. Sect. F Struct. Biol. Cryst. Commun.* **2017**, *73*, 235–240. [[CrossRef](#)] [[PubMed](#)]
52. Bommer, M.; Coates, L.; Dau, H.; Zouni, A.; Dobbek, H. Protein crystallization and initial neutron diffraction studies of the photosystem II subunit psbo. *Acta Crystallogr. Sect. F Struct. Biol. Cryst. Commun.* **2017**, *73*, 525–531. [[CrossRef](#)] [[PubMed](#)]
53. Coates, L.; Robertson, L. Ewald: An extended wide-angle laue diffractometer for the second target station of the spallation neutron source. *J. Appl. Crystallogr.* **2017**, *50*, 1174–1178. [[CrossRef](#)] [[PubMed](#)]



© 2018 by the authors. Licensee MDPI, Basel, Switzerland. This article is an open access article distributed under the terms and conditions of the Creative Commons Attribution (CC BY) license (<http://creativecommons.org/licenses/by/4.0/>).